

Effect of KCl on high-temperature corrosion of low-alloyed steel under low oxygen partial pressure

Alice Moya Núñez  | Rikard Norling 

Division of Materials and Production,
Department of Corrosion, RISE Research
Institutes of Sweden, Kista, Sweden

Correspondence

Rikard Norling, RISE Research Institutes
of Sweden, 16407 Kista, Sweden.
Email: rikard.norling@ri.se

Funding information

Swedish Energy Agency

Abstract

Low oxygen environments in biomass gasification and the presence of chlorine in feedstocks can influence the corrosion rate of steel by affecting the formation of protective oxide scales. The effect of KCl on the high-temperature corrosion of low-alloyed steel (13CrMo4-5) under low oxygen partial pressure is investigated by KCl salt spray ($0.1 \text{ mg}\cdot\text{cm}^{-2}$) and exposure to 3 vol% $\text{H}_2 + 30 \text{ vol}\% \text{H}_2\text{O} + \text{Ar}$ (balance) at 500°C for up to 168 h. Specimens without KCl salt are exposed for reference. Specimens are characterized after exposure by mass change, SEM/EDS, and XRD. KCl-deposited specimens exhibit about 30% lower mass gain after exposure compared to non-sprayed specimens. Their scale shows a porous innermost layer and a denser layer on top. No Fe or Cr chlorides are identified. The specimens without salt exhibit a similar two-layered scale, with a porous inner Fe-Cr oxide, followed by a denser and thicker Fe-oxide above. KCl could potentially protect the surface from further degradation by physically covering the specimen, altering the scale morphology, and forming a less permeable barrier, hindering the transport of species through the scale.

KEYWORDS

biomass, gasification, high temperature corrosion, potassium chloride, reducing atmosphere, steel

1 | INTRODUCTION

Overall energy consumption worldwide has rapidly increased over the last few decades and it is expected to continue growing, which could pose a threat to the energy transition target. Reducing the reliance on fossil fuels and maintaining and increasing the energy efficiency of present-day power plants are key activities to aid in this transition. An important renewable source

is biomass, which has directly contributed to the energy production sector as well as the production of bio-based fuels. Solid biomass can be converted to gas or liquid fuels through biochemical and thermochemical processes. Biomass gasification, in particular, is an attractive process as it allows the use of low-value feedstocks, such as agricultural and forestry waste.^[1–3] This process involves heating the raw materials to temperatures often between 800°C and 850°C , in specially designed plants,

Alice Moya Núñez and Rikard Norling contributed equally to this study.

This is an open access article under the terms of the [Creative Commons Attribution](https://creativecommons.org/licenses/by/4.0/) License, which permits use, distribution and reproduction in any medium, provided the original work is properly cited.

© 2024 RISE Research Institutes of Sweden AB. *Materials and Corrosion* published by Wiley-VCH GmbH.

that is, gasifiers, that allow the injection of oxygen and steam to produce syngas.^[4] Compared to traditional fossil fuels, biomass generally contains a higher amount of alkali metals, chlorine, and water, with a lowered concentration of sulfur.^[5–7] These differences can have important effects on metallic materials in combustion^[5,8] and gasification^[9–11] plants, for example, a higher risk of chlorine-induced corrosion. An additional challenge in biomass gasification is the low partial pressure of oxygen combined with high water contents, conditions that have been studied in laboratory conditions and shown to induce higher corrosion rates in a Cr-alloy^[12] and AISI 304L stainless steel^[13] compared to oxygen-containing atmospheres. The reducing atmosphere could interfere with the formation of stable and protective oxide layers, leading to rapid deterioration due to the high chlorine content in biomass-based feedstocks.^[10,14] Several research groups have performed laboratory studies in stainless and low-alloyed steels regarding their corrosivity in environments relevant to combustion and gasification of biomass, with the aim of elucidating mechanisms that allow for the use of lower cost and readily available materials for this application. In oxidative environments, Folkesson et al.^[15] have studied the addition of small amounts of KCl on the high-temperature corrosion of low-alloyed steel at 500°C, resulting in thicker scales for the KCl-deposited samples. The same alloy was studied at 400°C in oxidative conditions, reporting that KCl induced increased corrosion compared to PbCl₂ salt and the reference case without chloride salt.^[16] Jonsson et al. have studied the effect of KCl (s) on AISI 304L in oxidative environments, reporting the breakdown of the protective oxide scale.^[17] In low oxygen partial pressures, Elger et al.^[18] have exposed stainless steels in a simulated gasification environment at 600°C, resulting in the formation of thin and adherent chromium oxide layers and modest mass gain even when HCl(g) was present. However, the combined effect of KCl and low oxygen partial pressures, on the high-temperature corrosion of low-alloyed steels has not, to the best of our knowledge, been researched in controlled laboratory studies.

2 | MATERIALS AND METHODS/EXPERIMENTAL

The main material used for these exposures was low-alloyed steel ASTM T12, see Table 1 for composition. Other commercial higher-grade alloys (AISI 304L, Kanthal® APMT, Sanicro® 31HT, AISI 310S/310H) were exposed to the same atmosphere and conditions for comparison.

The specimens were cut in coupons of dimensions 15 mm × 10 mm × 3 mm. A small chamfer was ground on each specimen on the top right corner, to allow easy identification of the orientation of the sample. The samples were ground with silicon carbide paper up to P1200 grit and then ultrasonically cleaned in an ethanol/acetone bath for 20 min. The KCl salt mixture was prepared using 80 vol% ethanol (99.9%), 20 vol% deionized water, and enough KCl to saturate the solution. The mixture was stirred for 8 h using a magnetic stirrer and was left to settle overnight. The mixture was then applied to both sides of each sample, resulting in a deposited amount of KCl equivalent to $0.1 \pm 0.02 \text{ mg}\cdot\text{cm}^{-2}$ ($1.35 \pm 0.27 \mu\text{mol K}^+\cdot\text{cm}^{-2}$) confirmed by weighing. The samples were dried and then weighed using a five-digit microbalance. For the reference run, the samples were not sprayed with KCl.

The samples were placed in cylindrical alumina crucibles and inside a tube furnace (see Figure 1). The alumina crucibles had a small slit to allow gas flow and they were heat treated for 24 h at 1000°C before the exposures. At the start of the exposures, the tube furnace was flushed with Ar overnight. The temperature was then ramped to the target test temperature of 500°C ($\pm 3^\circ\text{C}$), and at around 200°C the water pump used to humidify the gas was turned on (deionized water). The experiments were carried out using a gas atmosphere composed of 3 vol% H₂ + 30 vol% H₂O + Ar (balance) with a flow rate of dry gas of 105 normal-ml·min⁻¹. The gas composition was set to resemble in a simplified manner that of a process gas in a gasification plant. The test temperature was set to represent a reasonable metal

TABLE 1 Nominal composition in wt% of alloys used in the exposures.

Alloy	C	Al	Si	Ti	Cr	Mn	Ni	Cu	Mo	Fe
ASTM T12 (HT5, 13CrMo4-5, 1.7335)	0.10	-	0.25	-	1.0	0.5	-	-	0.5	Bal.
AISI 304L (Alleima® 3R12)	≤0.03	-	0.5	-	18.5	1.3	10	-	-	Bal.
Kanthal® APMT	≤0.08	5.0	≤0.7	-	21.0	≤0.4	-	-	3.0	Bal.
Sanicro® 31HT (UNS N08811)	0.07	0.5	0.6	0.5	20.5	0.6	30.5	-	-	Bal.
AISI 310S/310H (Alleima® 7RE10)	0.06	-	≤0.75	-	24.5	1.5	21.0	-	-	Bal.

temperature of cooled components, such as heat exchangers, if they were to be placed in the gas flow path. The calculated oxygen partial pressure of the exposure gas was $p(\text{O}_2) = 2 \cdot 10^{-26}$ atm. At the exposure temperature, this condition allows for the formation of Fe_3O_4 but not Fe_2O_3 .^[19] Hence, the gas can be considered moderately reducing. The exposures were performed for 24 and 168 h. The crucibles were placed in a line following the direction of the gas flow. Triplicates of each material were used.

The corrosion products were analyzed using X-ray diffraction using a Bruker D8 Discover diffractometer with a copper $K\alpha$ beam of 1.5418 Å. The data was collected between 10° and 100° (2θ). Peak identification was done using the crystallography open database (COD). The corrosion products were characterized using a scanning electron microscope SEM (Zeiss Sigma VP 300), equipped with energy dispersive spectroscopy EDS (X-maxN).

3 | RESULTS

Figure 2 shows the gross mass gains for all the materials, including the reference alloys. In contrast to the result for the low-alloyed steel, the exposures resulted in no discernable mass changes for the higher alloyed reference materials when comparing the KCl-sprayed samples to the reference non-sprayed samples. The mass gain for the higher alloys was approximately of the same order of magnitude and almost negligible, while the mass gain for the low-alloyed steel samples was significantly higher. A magnification of this plot is shown in Figure 3, only for the low-alloyed steel samples. The KCl-sprayed low-alloyed steel samples showed less mass gain compared to the non-KCl ones. The mass gain of these samples is plotted against time in Figure 4, indicating that the mass gain for KCl-sprayed samples approximately follows a parabolic behavior from an early stage of the exposures.

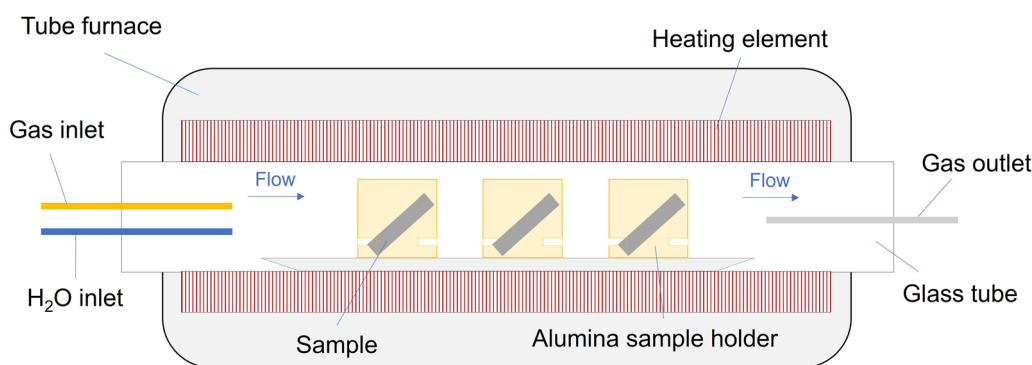


FIGURE 1 Schematic of tube furnace and triplicate sample setup inside alumina crucibles. Image not to scale. [Color figure can be viewed at wileyonlinelibrary.com]

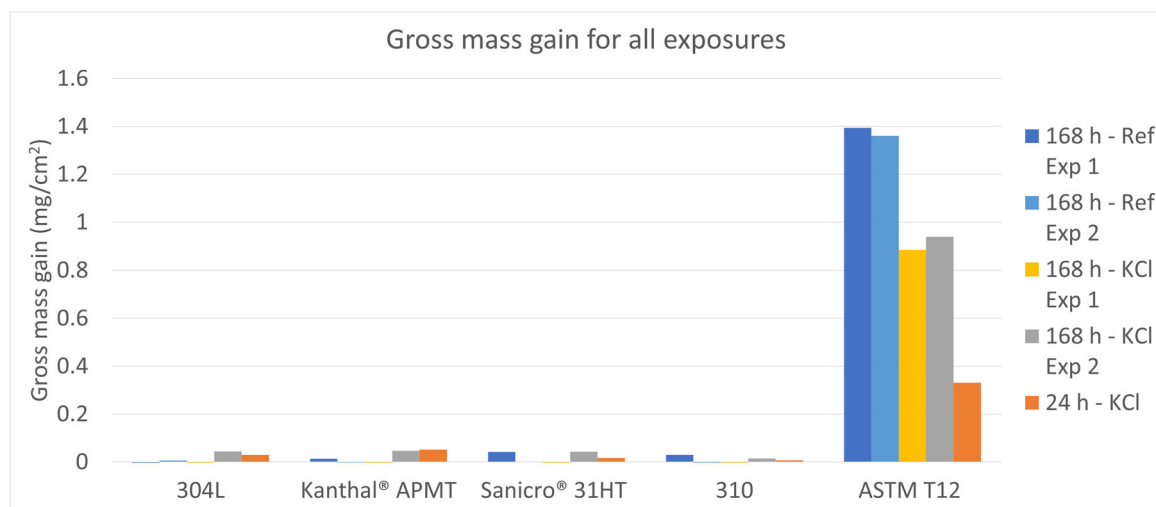


FIGURE 2 Gross mass gain for all exposures, including higher alloyed materials for comparison purposes. All higher alloyed materials had small mass gains of around the same order of magnitude. The low-alloyed steel sample exhibited a considerably higher gross mass gain. The reference exposure (without KCl salt) showed a larger gross mass gain than the KCl-sprayed specimens. [Color figure can be viewed at wileyonlinelibrary.com]

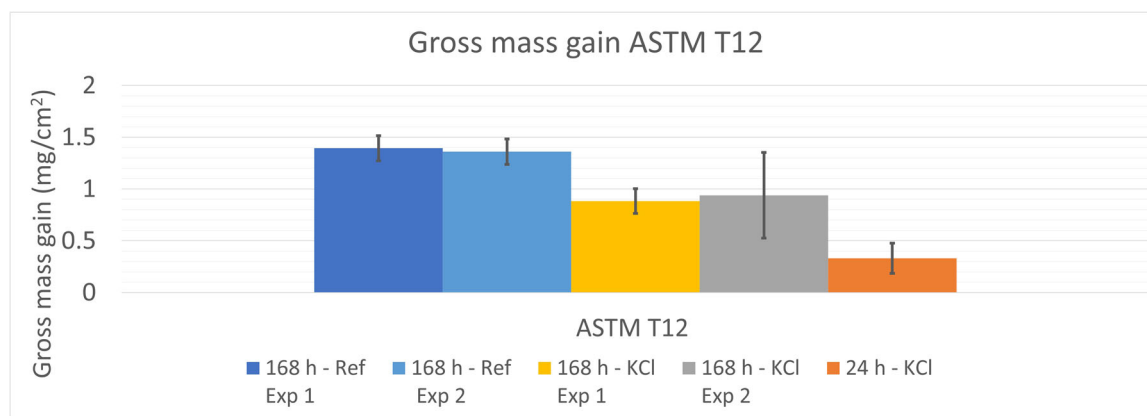


FIGURE 3 Gross mass gain for low-alloyed steel specimens. The bars include the standard deviation of triplicate samples. [Color figure can be viewed at [wileyonlinelibrary.com](https://onlinelibrary.wiley.com)]

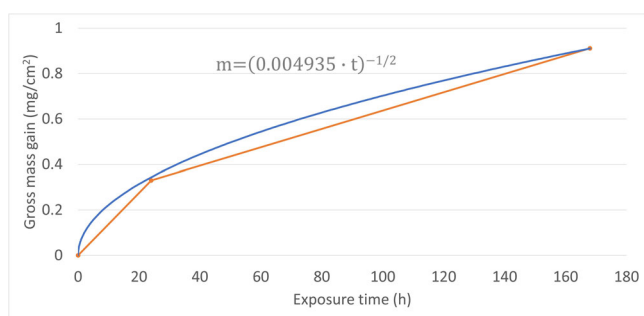


FIGURE 4 Plot of gross mass gain versus exposure time for the KCl salt exposures of the low-alloyed steel. The results have been fitted with a parabolic function. [Color figure can be viewed at [wileyonlinelibrary.com](https://onlinelibrary.wiley.com)]

The microstructure of the cross sections was examined, showing scale thickness differences that are in line with the mass gain results. Figure 5 shows an overview of the cross sections of the low-alloyed steel samples, exposed with and without the presence of KCl spray. The corrosion scale of the non-sprayed specimen exposed for 168 h is observed to be about 30% thicker than the corresponding sprayed one. The corrosion scale of specimens from the 168 h reference exposure without salt was characterized by a two-layered structure. The innermost layer was composed of a Cr-enriched iron oxide exhibiting a porous appearance (Figure 6). Above this layer, an iron-based oxide was observed, which was less porous, more homogeneous, and thicker compared to the innermost oxide layer.

The corrosion scale of KCl-sprayed samples exposed for 168 h was also characterized by a two-layered structure (see Figure 7), with relatively larger pores and a thinner scale than the reference specimen. The KCl sprayed samples exposed for 24 h exhibited a thinner two-layered structure, with smaller grains near the metal interface and large elongated (columnar) grains on top. Through EDS analysis

of the 168 h sprayed specimens, the elements Cl and K were found near the metal-oxide interface and in vertical channels extending to the surface of the scale (Figure 7). The atomic ratios of Cl and K were approximately 1:1, see Figure 8 and Table 2. Iron and chromium chlorides were not identified using XRD (see Figure 9) nor was there any indication of them by EDS analysis. The SEM-EDS and XRD results combined showed that the inner and outer oxide layers consisted of $(\text{Fe,Cr})_3\text{O}_4$ and Fe_3O_4 , respectively.

4 | DISCUSSION

The results show that KCl does not induce a more severe corrosion attack on low-alloyed steel samples compared to the reference non-sprayed samples. In oxidative environments, KCl has been shown to increase the corrosion rate of steels^[15] at equivalent temperatures compared to the present study. Additionally, eutectic mixtures of alkali salts have been studied in reducing environments showing increased corrosion rates, explained mostly by the low melting point of the mixtures. In that case, the initial states of degradation were most likely driven by the presence of molten salts.^[20] In the present study, contrary to the possible expectation that the alkali salt would induce harsher conditions for the exposed specimens in reducing environments, KCl-sprayed samples had a mass change about 30% lower than the non-sprayed samples, indicating that the presence of KCl deposit had a somewhat protective effect against corrosion. The mass loss of the sprayed samples follows a parabolic behavior; the rate of reaction is inversely proportional to the mass gain, represented by the well-known equation derived by Wagner^[21]:

$$\frac{dm}{dt} = \frac{K_p}{m}, \quad (1)$$

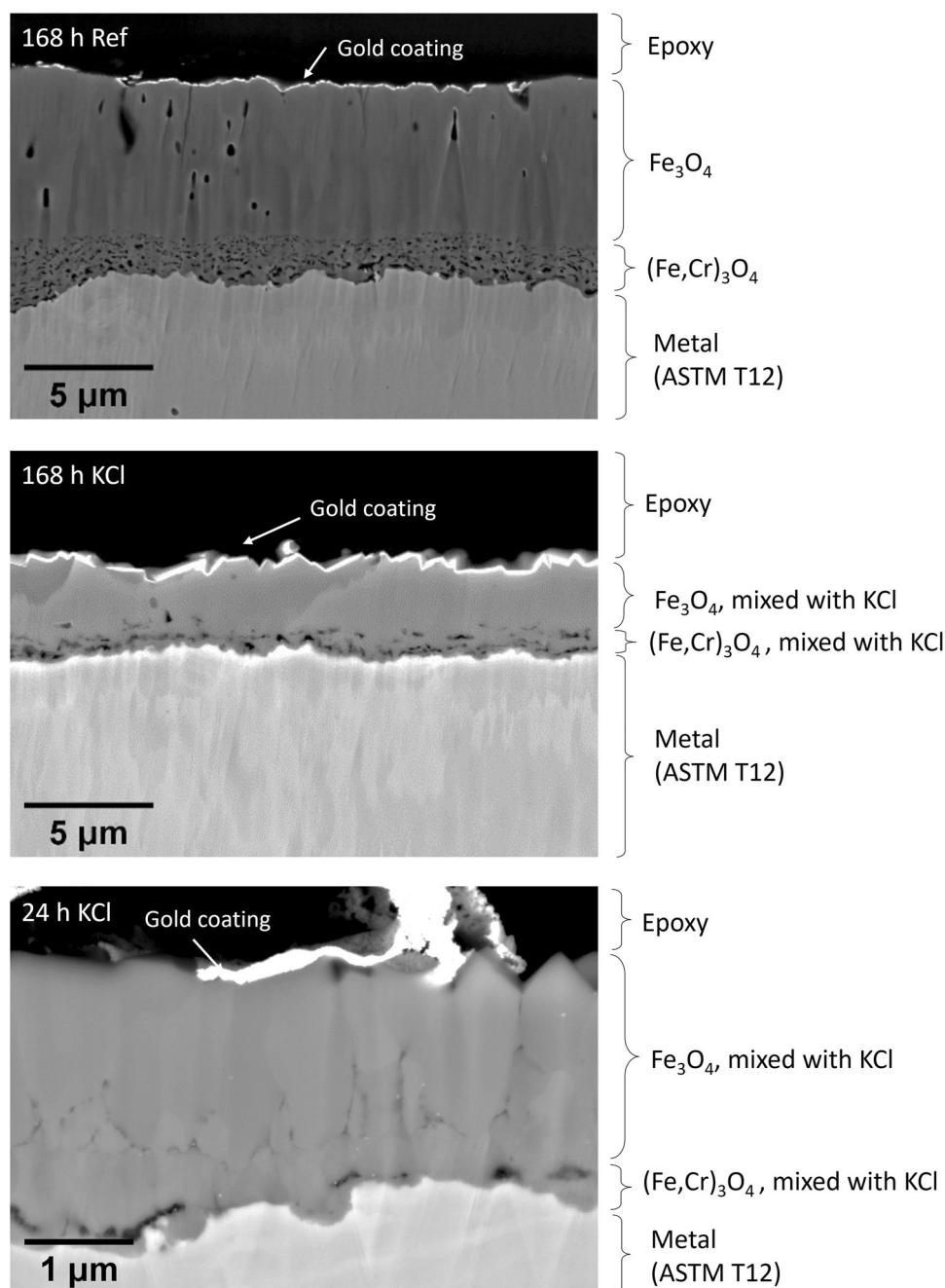


FIGURE 5 Backscatter SEM images of the reference sample without KCl (168 h), and the KCl-sprayed samples exposed for 168 and 24 h, respectively, for the low-alloyed steel.

where m is mass gain, t is time, and K_p is the parabolic rate constant.

The parabolic behavior (Figure 4) is in line with the observed progression of the scale thickness, from the 24 h to the 168 h exposure. The oxide layer growth rate thus decreases over time, suggesting a diffusion-controlled mechanism taking place. Thus, the presence of KCl did not have an effect on accelerating the corrosion rate of the low-alloyed steel.

With respect to possible interactions between the low-alloyed steel surface and KCl salt, there was no indication by XRD analysis that iron or chromium chlorides had formed. Moreover, the visible channels and pores in the EDS maps contained the elements Cl and K in atomic ratios of approximately 1:1, which gives additional evidence that base metal chlorides were not formed. If, for example, a volatile base metal chloride such as FeCl_3 had formed and had been

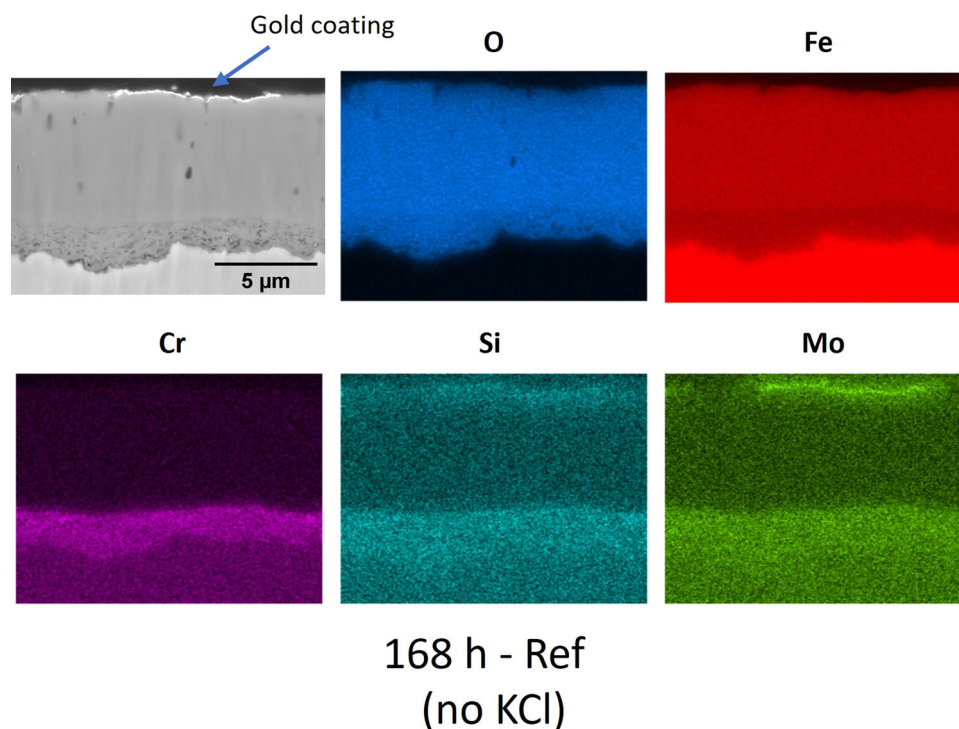


FIGURE 6 EDS analysis of a reference low-alloyed steel specimen, exposed to 3 vol% H₂ + 30 vol% H₂O + Ar (balance) for 168 h at 500°C. [Color figure can be viewed at [wileyonlinelibrary.com](https://onlinelibrary.wiley.com/doi/10.1002/maco.202414314)]

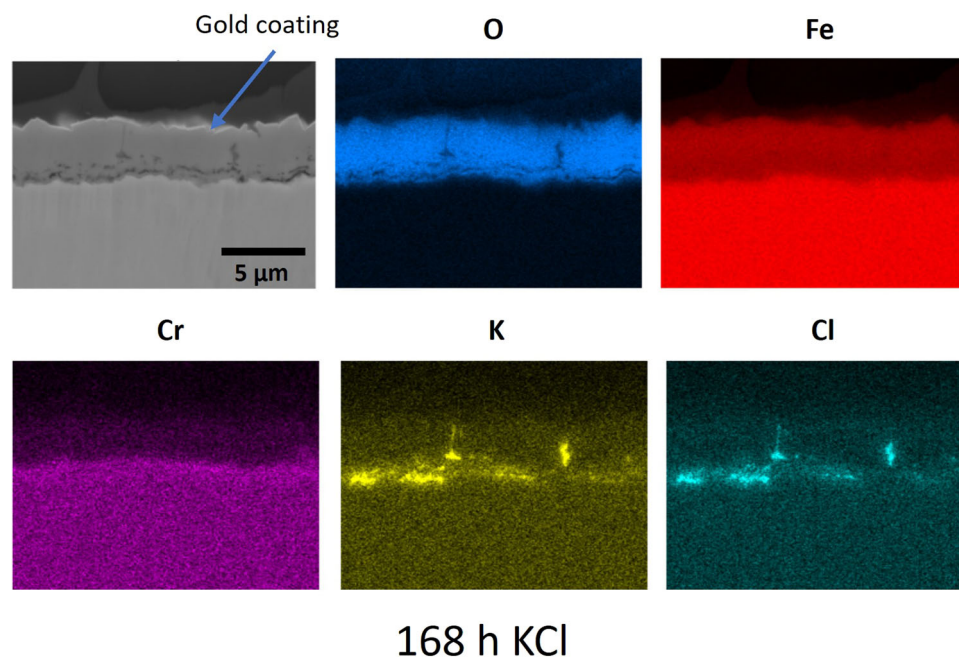


FIGURE 7 EDS analysis of a low-alloyed steel specimen sprayed with KCl and exposed to 3 vol% H₂ + 30 vol% H₂O + Ar (balance) for 168 h at 500°C. [Color figure can be viewed at [wileyonlinelibrary.com](https://onlinelibrary.wiley.com/doi/10.1002/maco.202414314)]

evaporated from the specimen in significant amounts, it would be expected that the Cl to K ratio should have been less than unity. The XRD results show for both types of exposures the presence of a spinel (either magnetite or a Fe-Cr spinel) and unreacted KCl for the KCl exposures. Hematite was not identified, indicating

that a moderately reducing atmosphere was achieved during the exposures.

The examined cross-sections show a slight difference between sprayed and non-sprayed samples. The appearance of the oxide layer of KCl-sprayed samples exhibited less overall porosity than the non-sprayed samples. These

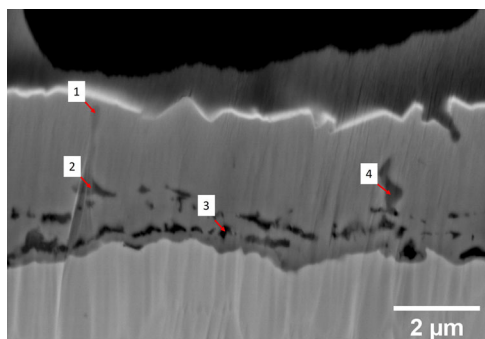


FIGURE 8 Backscatter SEM image of KCl-sprayed low-alloyed steel specimen, exposed to 3 vol% H₂ + 30 vol% H₂O + Ar (balance) for 168 h at 500°C. [Color figure can be viewed at [wileyonlinelibrary.com](https://onlinelibrary.wiley.com/doi/10.1002/maco.202414314)]

TABLE 2 EDS point analysis in at% of the areas in the cross-section in Figure 8.

Spectra	O	Fe	Cr	K	Cl	Si	Mo
Spectrum 1	38.55	74.59	0.0	4.94	4.86	0.0	
Spectrum 2	38.64	33.68	0.0	15.18	13.50	0.49	
Spectrum 3	51.47	35.99	6.97	1.92	1.92	1.23	0.49
Spectrum 4	37.53	33.87	0.0	14.14	14.46	0.0	

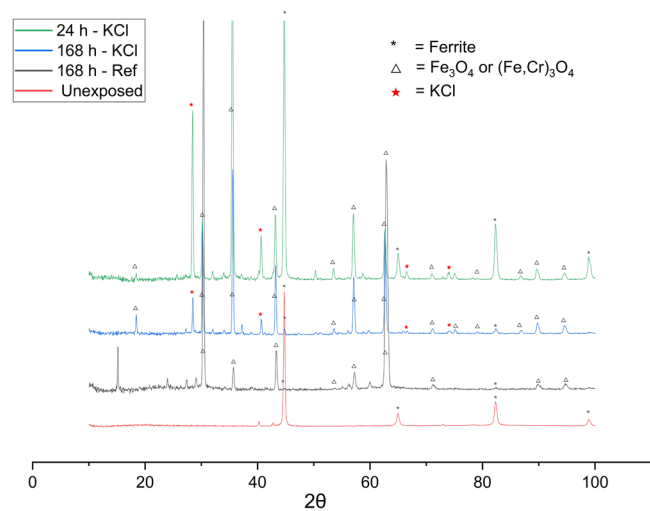


FIGURE 9 XRD patterns of low-alloyed steel specimens: exposed with KCl spray, reference, and unexposed. [Color figure can be viewed at [wileyonlinelibrary.com](https://onlinelibrary.wiley.com/doi/10.1002/maco.202414314)]

pores appear to be larger and localized for the most part at the interface of the inner oxide and the base metal. The appearance of the oxide layers in both sprayed and non-sprayed low-alloyed steel specimens suggests a similar growth mechanism, albeit at different rates. Elongated columnar grains were observed on top of a thinner chromium-containing layer, exhibiting smaller-sized grains. The appearance of the scale suggests a cationic

growth mechanism for the upper columnar layer and an anionic diffusion mechanism for the thinner innermost layer. The appearance and chemical composition of the innermost layer suggest an inward growth mechanism.

This type of layered structure is not unique and has been observed by other researchers on different steel grades, in both oxidative and reducing atmospheres. Folkesson et al.^[15] have observed a partially similar structure for low-alloyed steel in oxidative environments at the same exposure temperature of 500°C; however, observing the formation of an outermost layer of hematite due to the higher partial pressure of oxygen of said exposure. The layered structure in their non-KCl-deposited samples is equivalent to the non-KCl-sprayed samples in the present study; a porous inner layer corresponding to a spinel Fe and Cr-containing phase, followed by a thicker layer with large columnar magnetite grains, albeit exhibiting larger pores than the ones observed in the present study. This last difference can be attributed possibly to the formation of a dense outward-growing hematite layer, which could have been using the magnetite layer as a reservoir of iron cations when growing. The similarities end when comparing the KCl-deposited case. In the aforementioned study, a thicker and partially detached oxide layer was observed in the KCl-deposited samples. In addition, there was evidence of interaction of KCl with the steel, possibly through the formation of iron chlorides. The present study did not observe a thicker scale nor evidence of base metal chloride formation. In reducing atmospheres, Ardigo-Besnard et al.^[22] studied the high-temperature oxidation of commercial stainless steel without the presence of alkali salts. Their results suggest a cationic growth mechanism for the external magnetite layer and anionic for the chromium-containing spinel innermost oxide layer. The similarities with the appearance of the oxide layer in the present study suggest that the growth mechanism could be analogous to the aforementioned studies.

Indeed, the porosity observed in the innermost and finer-grained chromium-containing layer suggests the occurrence of a cationic diffusion mechanism that might have left voids behind (Kirkendall effect). The presence of hydrogen in the exposure environment could also have an effect on the diffusivity of iron. Murata et al.^[23] have observed that the diffusivity of Fe in (Fe,Cr)₃O₄ oxide scales is higher in the presence of hydrogen and generally higher than Cr, promoting the preferential outward diffusion of Fe, which might further explain the porous appearance of the innermost Cr-containing layer observed in the present study.

It is hypothesized that non-reacting KCl hindered to some extent the diffusion of iron cations from the spinel innermost layer toward the outer oxide, by possibly

physically covering the exposed surface of the substrate, thus the observed difference in scale thickness. Also, the scale morphology has been altered. Altogether, the formed oxides scale constitutes a less permeable barrier, hindering the transport of species through the scale. The non-interaction of the KCl salt with the metal substrate was indicated by not observing base metal chlorides, as well as with the negligible effect of the exposure in the higher reference alloys. The KCl was not observed to be interacting with the atmosphere either, evidenced by the negligible weight change observed in the higher alloyed materials.

5 | CONCLUSIONS

The effect of KCl on high-temperature corrosion under low oxygen partial pressure was investigated by exposures of specimens with and without KCl in 3 vol% H₂ + 30 vol% H₂O + Ar (balance) at 500°C for up to 168 h. The following conclusions were drawn from the results for these conditions:

- KCl does not induce aggravated corrosion in any of the tested alloys, including the low-alloyed steel ASTM T12.
- Iron chlorides were neither observed nor identified in the exposed samples and therefore concluded not likely to be formed.
- KCl could potentially protect the surface from further degradation by physically covering the specimen, altering the scale morphology, and forming a less permeable barrier, hindering the transport of species through the scale.

AUTHOR CONTRIBUTIONS

Alice Moya Núñez was involved in the investigation and writing—original draft, review, and editing. Rikard Norling was involved in conceptualization, project management, and writing—original draft, review, and editing.

ACKNOWLEDGMENTS

Eric Börjesson is gratefully acknowledged for performing valuable laboratory work. The work was performed within the Swedish High Temperature Corrosion Centre (HTC) and it was funded by the Swedish Energy Agency. Alleima (formerly Sandvik), Cortus Energy, Kanthal, and Phoenix Biopower are acknowledged as valuable project partners. Alleima (formerly Sandvik) and Kanthal are acknowledged for providing the test materials.

CONFLICT OF INTEREST STATEMENT

The authors declare no conflict of interest.

DATA AVAILABILITY STATEMENT

The data that support the findings of this study are available from the corresponding author upon reasonable request.

ORCID

Alice Moya Núñez  <https://orcid.org/0000-0001-6256-7123>

Rikard Norling  <http://orcid.org/0000-0002-2339-9443>

REFERENCES

- [1] E. R. Widjaya, G. Chen, L. Bowtell, C. Hills, *Renew. Sustain. Energy Rev.* **2018**, *89*, 184.
- [2] A. Kumar, D. Jones, M. Hanna, *Energies* **2009**, *2*, 556.
- [3] A. D. Korberg, B. V. Mathiesen, L. R. Clausen, I. R. Skov, *Smart Energy* **2021**, *1*, 100006.
- [4] Ö. Tezer, N. Karabağ, A. Öngen, C. Ö. Çolpan, A. Ayol, *Int. J. Hydrogen Energy* **2022**, *47*, 15419.
- [5] H. P. Nielsen, F. J. Frandsen, K. Dam-Johansen, L. L. Baxter, *Prog. Energy Combust. Sci.* **2000**, *26*, 283.
- [6] B. M. Jenkins, L. L. Baxter, T. R. Miles, T. R. Miles, *Fuel Process. Technol.* **1998**, *54*, 17.
- [7] A. Demirbaş, *Energy Sources* **2005**, *27*, 451.
- [8] A. A. Khan, W. de Jong, P. J. Jansens, H. Spliethoff, *Fuel Process. Technol.* **2009**, *90*, 21.
- [9] R. Elger, F. Lindberg, R. Norling, R. Pettersson, *Mater. High Temp.* **2015**, *32*, 36.
- [10] R. Källström, *J. Phys. IV* **1993**, *3*, C9-751.
- [11] J. Keiser, R. Connatser, M. Brady, S. Lewis, L. Donovan, in *NACE International Corrosion Conference Proceedings*, Houston, **2018**.
- [12] M. Hänsel, W. J. Quadackers, D. J. Young, *Oxid. Met.* **2003**, *59*, 285.
- [13] T. Jonsson, S. Karlsson, H. Hooshyar, M. Sattari, J. Liske, J.-E. Svensson, L.-G. Johansson, *Oxid. Met.* **2016**, *85*, 509.
- [14] W. T. Bakker, *Mater. High Temp.* **1997**, *14*, 197.
- [15] N. Folkesson, T. Jonsson, M. Halvarsson, L.-G. Johansson, J.-E. Svensson, *Mater. Corros.* **2011**, *62*, 606.
- [16] E. Larsson, H. Gruber, K. Hellström, T. Jonsson, J. Liske, J.-E. Svensson, *Oxid. Met.* **2017**, *87*, 779.
- [17] T. Jonsson, J. Froitzheim, J. Pettersson, J.-E. Svensson, L.-G. Johansson, M. Halvarsson, *Oxid. Met.* **2009**, *72*, 213.
- [18] R. Elger, R. Norling, R. Pettersson, *Mater. Corros.* **2016**, *67*, 939.
- [19] K. C. Sabat, A. B. Murphy, *Metall. Mater. Trans. B* **2017**, *48*, 1561.
- [20] T. J. Pan, C. L. Zeng, Y. Niu, *Oxid. Met.* **2007**, *67*, 107.
- [21] C. Wagner, *Z. Phys. Chem.* **1933**, *21B*, 25.
- [22] M. R. Ardigo-Besnard, I. Popa, O. Heintz, R. Chassagnon, M. Vilasi, F. Herbst, P. Girardon, S. Chevalier, *Appl. Surf. Sci.* **2017**, *412*, 196.
- [23] Y. Murata, H. Minai, K. Nagai, A. Shiraki, M. Morinaga, *ISIJ Int.* **2008**, *48*, 1434.

How to cite this article: A. Moya Núñez, R. Norling, *Mater. Corros.* **2024**, *1*–8. <https://doi.org/10.1002/maco.202414314>